Nanocrystalline diamond film growth on plastic substrates at temperatures below 100 °C from low-temperature plasma

Kazuo Tsugawa,* Masato Ishihara, Jaeho Kim, Yoshinori Koga, and Masataka Hasegawa†
Nanotube Research Center, National Institute of Advanced Industrial Science and Technology (AIST), Tsukuba Central 5, 1-1-1 Higashi, Tsukuba, Ibaraki 305-8565, Japan

(Received 2 April 2010; revised manuscript received 9 July 2010; published 30 September 2010)

Nanocrystalline diamond films have been successfully synthesized on plastic substrates at substrate temperatures below 100 °C using a microwave plasma chemical-vapor deposition technique. This has been realized by using low reaction-gas pressures and a surface-wave plasma with a low-electron temperature over the growth region. The nanocrystalline diamond films exhibit growth rates with much lower temperature dependence than conventional diamond growth and decreasing nucleation rates with increasing substrate temperatures. These phenomena imply a different growth mechanism from conventional diamond syntheses. In addition, our analysis on the crystal size distribution of the nanocrystalline diamond film indicates the possibility of diamond nucleation in a stable phase in the plasma. The gas-phase nucleation, invoked by the low-electron temperature of the surface-wave plasma, well explains the low-temperature growth and the temperature dependences of the growth rate and the nucleation rate.

DOI: 10.1103/PhysRevB.82.125460 PACS number(s): 68.55.ag, 68.55.aj, 81.15.Gh

I. INTRODUCTION

Diamond is very useful as an engineering material due to its superlative physical properties, such as the highest hardness and thermal conductivity of any bulk materials. Furthermore, exceptional aspects of its superb physical properties have gathered interest from a technological view point. For example, diamond is a unique electrical insulating material with high thermal conductivity, which is expected to solve the growing thermal problem in electronic devices (e.g., by using such as silicon-on-diamond substrates).[1]

For industrial use, in particular, diamond thin-film synthesis is important. Generally speaking, diamond thin films are synthesized by using a chemical-vapor deposition (CVD) technique. Typical substrate temperatures during the CVD process exceed 700 °C for conventional microcrystalline diamond (MCD) (Ref. 2) and 400 °C for nanocrystalline diamond (NCD).[3] These high substrate temperatures have limited the substrate materials that can be used for diamond film deposition. Thus, the low-temperature growth gives wide substrate selection, which will lead to many innovative new applications.

From this point of view, many efforts to lower the deposition temperature of diamond have been made.[4–10] Ong *et al.*[4] have developed a low-temperature diamond deposition process using microwave plasma CVD (MWPCVD) method in a pulsed mode. They reported diamond deposition on quartz substrates at average substrate temperatures of 400–600 °C. Muranaka *et al.*[5] have characterized diamond films grown on Si substrates by MWPCVD at substrate temperatures between 130 and 750 °C. Ihara *et al.*[6] have used hot-filament CVD (HFCVD) for low-temperature deposition of diamond on Si wafers. They obtained diamond particles on the substrate at a substrate temperature of 135 °C. Yara *et al.*[7] have reported diamond deposition at a substrate surface temperature of 200 °C using magnetoactive MWPCVD. Recently, Piazza and Morell[8] have reported nanocrystalline diamond growth on polyimide films at substrate temperatures of around 250 °C by using sulfur-assisted HFCVD. In our previous work,[9,10] we have deposited continuous NCD films on Si and glass substrates at substrate temperatures of 100–500 °C using a microwave surface-wave plasma. In spite of these attempts, conclusive evidence that a diamond film can grow at a substrate temperature as low as 100 °C has not been reported so far. Convincing evidence of diamond growth at even lower substrate temperatures than 100 °C will lead to the next generation of diamond applications in industry.

In this work, in an attempt to lower the substrate temperature during the diamond growth process using MWPCVD, we have successfully synthesized NCD films on plastic substrates at substrate temperatures below 100 °C. We have selected polyphenylene sulfide (PPS) as the substrate material, which is a widely used engineering plastic with the melting point of 285 °C. In hitherto known diamond CVD processes, plastic substrates have hardly been used due to high process temperatures of diamond synthesis.

The key technology for the low-temperature diamond deposition in this work is the use of the surface-wave plasma[11] in the MWPCVD process. It gives a stable plasma at a low-pressure reaction gas below 10^2 Pa and a low-electron temperature below 5 eV over the CVD growth region. These two points are essential for the low-temperature growth of diamond in the present work. We have used lower pressures of the reaction gas than those in conventional diamond CVD processes, which are effective in maintaining low substrate temperatures. In conventional diamond CVD processes, reaction-gas pressures of 10^3–10^4 Pa are used in general. In the present work, we have used much lower pressures of 2×10^1–4×10^2 Pa than those in conventional processes. At such low pressures, a plasma is hardly maintained using conventional MWPCVD systems. In contrast, the surface-wave plasma is maintained with stability at those low pressures. In addition, the surface-wave plasma has a low-electron temperature over the CVD region (bulk plasma region).[12,13] The low-electron temperature of the surface-

 ©2010 The American Physical Society

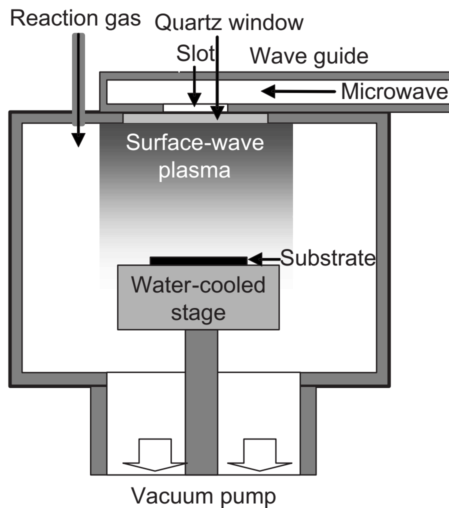

FIG. 1. Schematic illustration of the microwave plasma CVD system used for the low-temperature deposition of nanocrystalline diamond films.

wave plasma is efficient at suppressing excessive carbon decomposition that results in the presence of nondiamond components in the deposited film. Our plasma diagnoses have revealed that the electron temperature is 2.6 ± 0.5 eV in the CVD region while those in conventional MWPCVD process exceed 5 eV.[14,15]

II. EXPERIMENT

PPS plates with $50 \times 50 \times 2$ or $25 \times 25 \times 2$ mm^3 in size were used as substrates for CVD growth of NCD. Before the CVD treatments, the substrates underwent seeding pretreatments by using ethanol or water suspension with dispersed detonation nanocrystalline diamond powder of 5 nm in average crystal size. The suspension was spread on the substrate by using a spin coater or by using ultrasonication.

The low-temperature MWPCVD treatments were carried out in a reaction chamber with a slot type antenna on a waveguide attached to the top flange. A schematic illustration of the MWPCVD system is shown in Fig. 1. A microwave of 1.5 kW at 2.45 GHz is radiated from the slot and introduced into the chamber through a quartz window under the slot. A surface-wave-excited plasma is generated under the window. This MWPCVD system is different from the one used in our previous work,[9] which is equipped with antennas in quartz tubes for the surface-wave-plasma excitation. In the CVD process, reaction-gas pressures in the range of $2.0 \times 10^1 - 4.0 \times 10^2$ Pa were used. Plasma parameters such as plasma (electron) density n_e and electron temperature T_e of the plasma generated by the MWPCVD system were measured using a Langmuir double probe with hydrogen gas at pressures of 10–100 Pa. As a result, almost constant T_e around 2.6 ± 0.5 eV over the CVD region was obtained while T_e=4–9 eV at the plasma generation region (just under the quartz window). The CVD region is distant 85 mm below the window. The measured n_e exhibited $2-10 \times 10^{11}$ cm^{-3} at the plasma generation region, which is larger than the cutoff density $n_c = 7.4 \times 10^{10}$ cm^{-3} of a 2.45 GHz microwave plasma.[11] This indicates that the plasma is excited and sustained by surface waves along the window.

We adopted a $H_2+CH_4+CO_2$ gas mixture for the reaction gas. The same concentrations in the range of 5–20 % were used for CH_4 and CO_2. In general, reaction gas mixtures of hydrogen-diluted carbon source gas, CH_4 in most cases, are used in diamond CVD processes to remove nondiamond components in deposited films using etching by atomic hydrogen.[16] At low substrate temperatures such as below 600 °C, however, the atomic-hydrogen etching is insufficient to remove nondiamond components. Hence we introduced CO_2 into the reaction gas mixture to enhance the etching effect at low substrate temperatures by oxygen.[17–19]

We applied a water cooled substrate holder to maintain the substrate below 100 °C. The substrate temperature was monitored by a K-type thermocouple in contact with the substrate surface.

After the MWPCVD treatments, the deposited films on the substrates were characterized using Raman-scattering spectroscopy to confirm diamond formation, on a UV-excited Raman system JASCO NRS-1000 UV (excitation wavelength=244 nm, 100 mW). X-ray diffraction patterns of the films for the estimation of the average crystallite sizes were obtained using a Rigaku Rint Ultima III x-ray diffractometer with Cu $K\alpha$ radiation (wavelength=0.1542 nm, 40 kV, 40 mA). High-resolution transmission electron microscopy (TEM) images were taken on a Hitachi H-9000 TEM system with an acceleration voltage of 300 kV. Film thicknesses were measured optically on a Filmetric F20 thin-film thickness measurement system.

III. RESULTS

Figure 2 demonstrates the importance of lowering the substrate temperature, showing the effect of exposing the PPS substrate to a plasma at a temperature exceeding 100 °C. Figure 2(a) shows a PPS substrate before the exposure. The PPS substrate shown in Fig. 2(a) was exposed to a microwave plasma of a $H_2+CH_4+CO_2$ gas mixture in the CVD chamber under the same gas conditions as the NCD synthesis. When the substrate temperature exceeds 100 °C, the PPS substrate is damaged by the plasma, as demonstrated in Fig. 2(b). The white material in Fig. 2(b) is residuary filler that was present in the PPS substrate before the CVD process (the plastic decomposed during the process). In contrast to this, the PPS substrate does not suffer any appreciable damage when the substrate temperature is below 100 °C. Thus in order to avoid damage from the plasma, the substrate temperature is required to be maintained below 100 °C. This indicates that the hydrogen-plasma etching strongly depends on the substrate temperature.

Figure 3 shows a PPS substrate after the CVD treatment at a substrate temperature of around 80 °C without any noticeable damage. A color pattern by optical interference is observed on the PPS substrate in the picture, which indicates the formation of a transparent thin film. Figure 4 shows typical Raman-scattering spectra of films deposited on the PPS substrates using an excitation wavelength of 244 nm. Spectra from two films deposited for different duration of the CVD

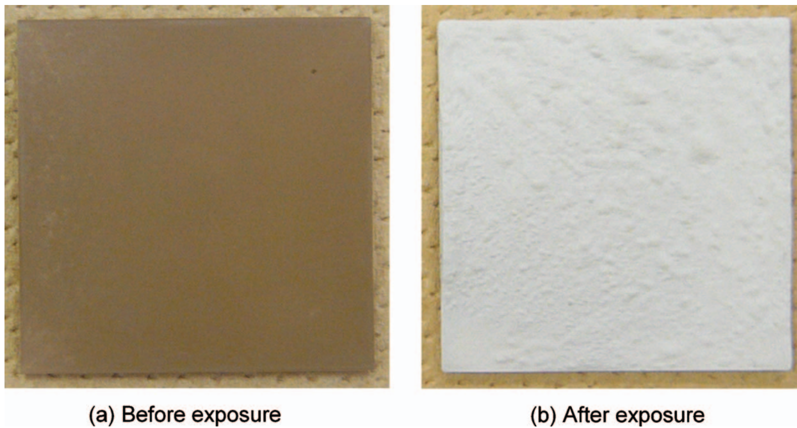

FIG. 2. (Color) Demonstration of damage to a PPS substrate by a plasma exposure. (a) A PPS substrate before a plasma exposure. (b) The PPS substrate after an exposure to a plasma of a H_2 $+CH_4+CO_2$ gas mixture in the CVD chamber at substrate temperatures from 145 to 167 °C for 5 min. The PPS substrate was damaged and decomposed by the plasma exposure, leaving white residuary filler shown in (b).

growth are demonstrated in the figure, i.e., 4 and 8 h. For comparison, a Raman spectrum of a PPS substrate without the CVD treatment is also shown in the figure. One can see clearly the signature of diamond at 1333 cm^{-1} in Raman shift. The intensity of the diamond peak increases with deposition time, indicating the growth of the diamond film in the CVD process.

Figure 5 demonstrates a typical x-ray diffraction pattern (using Cu $K\alpha$) of the diamond film on PPS. In the pattern, the peak of reflection from diamond (111) planes is observed at $2\theta=43.9°$ while an untreated PPS substrate exhibits no diffraction peak near that position. The average crystallite size of the film is estimated from the broadening of the diffraction peak of (111) by using the Scherrer equation.[20] The inset of Fig. 5 depicts the (111) diffraction peak fitted by the Pearson VII function.[21] We have used the full width at half maximum of the fitted Pearson VII function, and consequently the average crystallite size is approximately 5.5 nm. This indicates that the film on the PPS substrate consists of nanocrystalline diamonds.

IV. DISCUSSION

A. Growth rate

In order to analyze the mechanism of the NCD deposition at temperatures below 100 °C, first, growth rates are estimated. The growth rate r is defined as film thickness grown per unit time. Hence $r=L/t$, where L and t, respectively, are the film thickness and the deposition time (duration of the CVD treatment). The growth rates r of NCD films in the present work have been estimated from experimentally obtained L and t. Figure 6 displays the growth rates of NCD films on PPS, stainless steel, silicon (Si), and sintered tungsten carbide (WC) substrates at various substrate temperatures, deposited by the microwave surface-wave plasma CVD system using the same gas mixture and pressure (20 Pa). The substrate temperatures range below 100 °C for the PPS, around 470 °C for the stainless steel, 500–600 °C for the Si, and around 700 °C for the WC substrates. Typical growth rates of MCD (Ref. 22) and ultrananocrystalline diamond (UNCD) (Ref. 3) are also indicated in the figure.

Assuming that the growth rate does not depend on the substrate material, the activation energy of the growth rate is derived from the temperature dependence of the growth rates (Arrhenius plots). Suppose the growth rate r is related to the substrate temperature T by an Arrhenius-type form $r \propto \exp(-E_a/k_BT)$, where E_a is derived from the gradient of a least-square fit among the growth rates. Here k_B denotes the Boltzmann constant. In the case of Fig. 6, the derived E_a is 0.069 ± 0.012 eV. This value is much lower than typical ac-

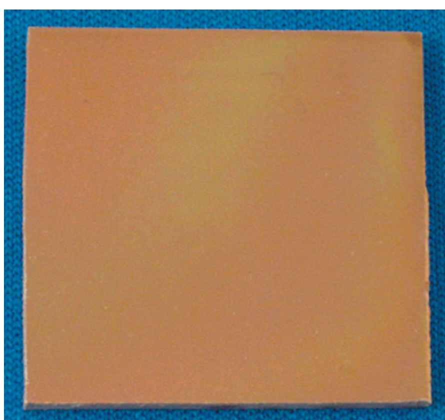

FIG. 3. (Color) PPS substrate after the CVD process at a substrate temperature below 100 °C (around 80 °C). A color pattern can be seen on the surface, indicating formation of a transparent film.

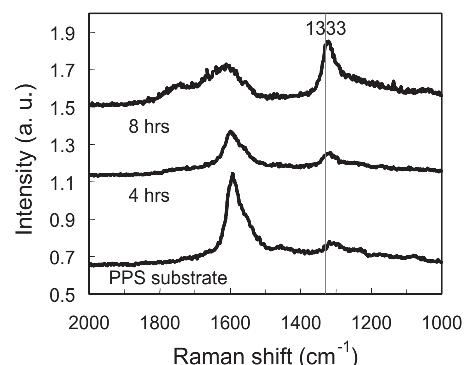

FIG. 4. Typical Raman spectra of films deposited on the PPS substrates using an excitation wavelength of 244 nm. Spectra from two films via different durations of the CVD growth displayed, i.e., 4 and 8 h. A typical spectrum of a bare PPS substrate before the CVD treatment is also shown. The peak around 1333 cm^{-1} in Raman shift indicates the diamond signature, the intensity of which increases with increasing duration of the CVD treatment.

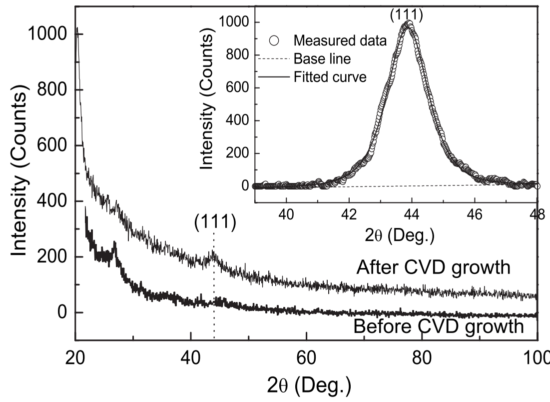

FIG. 5. Typical x-ray diffraction pattern of a diamond film deposited on PPS using Cu $K\alpha$. The duration time of the CVD growth is 8 h and the thickness of the deposited diamond film is around 500 nm. A diffraction pattern from a PPS substrate without the CVD growth is also shown for comparison. A diffraction peak at $2\theta=43.9°$ from the reflections of diamond (111) is observed in the pattern from the CVD-treated PPS substrate (indicated by "after CVD growth") while no peak is observed around that position in the pattern from the PPS substrate with no growth (indicated by "before CVD growth"). The inset shows the magnified (111) peak with a fitted curve with background elimination. The dashed line in the inset denotes a base line.

tivation energies of UNCD [0.254 ± 0.019 eV (Ref. 3)], conventional MCD [1.00 ± 0.05 eV (Ref. 22)], and homoepitaxial single-crystalline diamond (0.3 ± 0.1, 0.78 ± 0.09, and 0.52 ± 0.17 eV for [100], [110], and [111] growth, respectively[23]). In a similar style to Robertson,[24] Fig. 6 shows a comparison of the temperature dependence of growth rates among the MCD,[22] the UNCD,[3] and the NCD in the present work. The differences of the activation energies are clearly observed in the figure. The result implies that the growth mechanism of the NCD in the present work is different from that in the MCD or in the UNCD growth.

For further analysis of the growth mechanism, the nucleation rate is estimated. In the present work, the average crys-

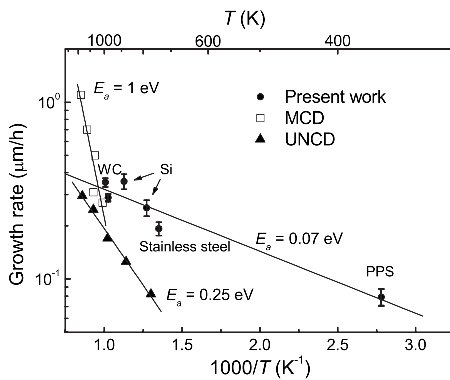

FIG. 6. Temperature dependence of growth rates. In addition to the growth rate of the nanocrystalline diamond in this work, typical growth rates of microcrystalline diamond (Ref. 22) and ultrananocrystalline diamond (Ref. 3) are also shown for comparison. Vertical error bars indicate standard errors coming from uncertainty in the determination of film thicknesses.

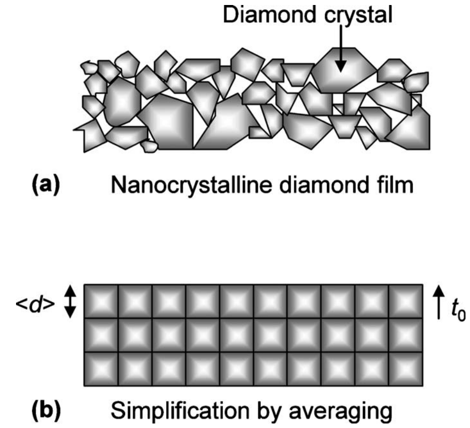

FIG. 7. Schematic of modeling to estimate nucleation rates. (a) A NCD film is simplified into a film constructed from diamond crystals with a uniform size $\langle d\rangle$ (average crystal size) (b). On average, the NCD film grows to $\langle d\rangle$ in thickness in a time t_0, i.e., the growth rate r is described as $r=\langle d\rangle/t_0$.

tallite size obtained from x-ray diffraction is independent of the film thickness, i.e., the average crystallite size is almost constant regardless of the film thickness. This indicates that the size distribution of diamond crystals does not change considerably from near the substrate to the surface of the film like the UNCD film.[25] This fact suggests the constant occurrence of diamond renucleation on the surface of the growing NCD film during the CVD process.[25] In contrast to this situation in general, typical MCD films consist of columnar grains. This type of morphology indicates that the diamond nucleation occurs on the substrate surface and the nucleated grains continue to grow throughout the deposition process.

B. Nucleation rate

Considering the discussion above, nucleation rates of the NCD growth are estimated by using a simple growth model. To simplify the estimation, we assumed a constant nucleation rate per unit area per unit time, ν, for a given substrate temperature. Furthermore, each nucleated diamond crystal on the growing diamond film surface is assumed to grow up to the mean crystal diameter $\langle d\rangle$, i.e., the diamond film is constructed from diamond crystals with a uniform size of $\langle d\rangle$. In addition, nucleation is assumed to occur randomly on the growing surface and the diamond film grows layer by layer on average. This model of the growing diamond film is depicted schematically in Fig. 7.

Using this simple model, the nucleation density per unit area, n, is described as $n=1/\langle d\rangle^2=\nu t_0$. Here t_0 is the time for which a layer with a thickness of $\langle d\rangle$ grows. In addition, the growth rate of a film r can be written as $r=\langle d\rangle/t_0(=L/t)$. Hence the nucleation rate ν is given by

$$\nu=\frac{r}{\langle d\rangle^3}. \quad (1)$$

Here, L, t, and $\langle d\rangle$ are obtained experimentally. Thus, the growth rates r and the nucleation rates ν are evaluated by using these experimental values.

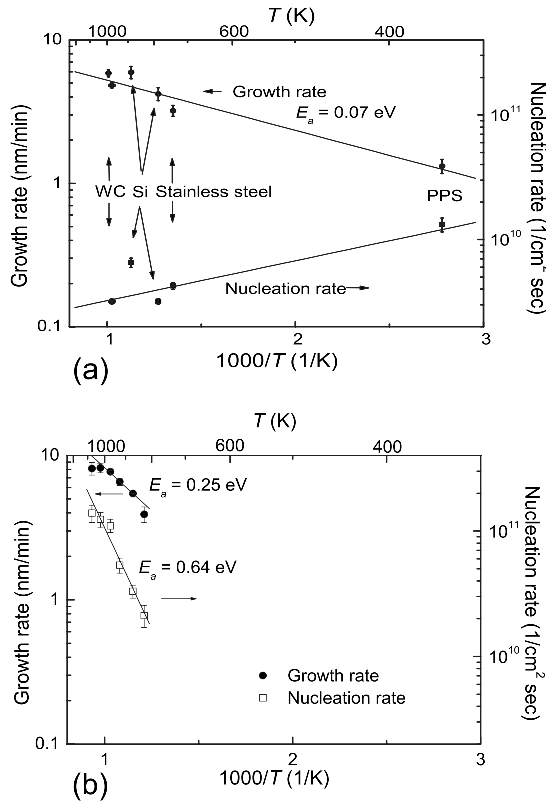

FIG. 8. Temperature dependence of growth rates and nucleation rates of (a) nanocrystalline diamond films in this work and of (b) ultrananocrystalline diamond in Ref. 26, plotted in the same scales for comparison. In (a), three kinds of substrates were used for specific substrate temperature ranges, namely, PPS for below 100 °C, stainless steel for around 470 °C, silicon (Si) for 500–600 °C, and sintered tungsten carbide (WC) for around 700 °C. In (b), the plotted data are calculated using experimental data taken from Ref. 26.

Estimated nucleation rates, ν, versus reciprocal temperature are shown in Fig. 8(a) along with the growth rates, using average crystallite sizes obtained from x-ray diffraction measurements as $\langle d \rangle$. Generally speaking, the mechanism of crystal growth can be divided sequentially into two stages, namely, nucleation and growth of the nuclei. In the present work, from Fig. 8(a), the nucleation rate decreases with increasing substrate temperature T. This tendency is in contrast with conventional nucleation, where the nucleation rate increases along with temperature. In fact, in UNCD growth, for example, the nucleation rate increase with increasing substrate temperature as demonstrated in Fig. 8(b).

Figure 8(b) shows Arrhenius plots of growth rates and nucleation rates of UNCD film growth in HFCVD.[26] The plotted data were calculated from experimental data in Ref. 26 in the same manner as the present work. The nucleation rate of the UNCD growth in Fig. 8(b) increases with increasing substrate temperature with an activation energy of 0.64 eV, exhibiting a similar trend to the growth rate. This type of temperature dependence of the nucleation rate coincides with the conventional nucleation. On the other hand, in the NCD growth in the present work in Fig. 8(a), the nucleation rate seems not to be thermally activated. It decreases with increasing substrate temperature. In other words, the NCD growth is hardly explained by a model based on the conventional nucleation at the substrate surface. This suggests that the nucleation occurs in the surface-wave plasma via a different mechanism from that of usual nucleation.

C. Growth mechanism

Generally speaking, the texture structure of a thin film reflects its history of growth. The morphologies and the dimensions of grains or crystallites in the film therefore give a fingerprint of the growth mechanism. From this point of view, we have investigated crystal size distribution of a NCD film synthesized on a PPS substrate at a substrate temperature of ~86 °C, in order to analyze the nucleation and the growth mechanism further. The size distribution has been obtained from a high-resolution TEM image shown in Fig. 9(a). The obtained size distribution is presented in Fig. 9(b). From this figure, the NCD film is found to consist of spherical diamond crystals ranging from 3 to 10 nm.

In the current investigation, it was determined experimentally that the surface roughness does not depend on the film thickness, which indicates that there is no correlation between successive nucleation events. Therefore, a Poisson process, with nucleation at a constant rate ν, can be utilized.

The probability $P_r[N(t+\tau)-N(t)=k]$ of the number of nucleation occurrences $N(t+\tau)-N(t)=k$ in a time interval $(t,t+\tau]$ at a nucleation site with a mean area $\langle d\rangle^2$ is expressed by a Poisson distribution $P(k;\nu\langle d\rangle^2\tau)$ as

$$P_r[N(t+\tau)-N(t)=k] = P(k;\nu\langle d\rangle^2\tau) = \frac{(\nu\langle d\rangle^2\tau)^k e^{-\nu\langle d\rangle^2\tau}}{k!},$$

$$k=0,1,\ldots$$

Next, the distribution of the time interval between successive nucleation occurrences τ is derived. Supposing no nucleation occurs in the time interval τ and one nucleation occurs in the next small interval $d\tau$, the total probability is obtained as a product of two Poisson distributions due to the independence between the two events as follows:

$$P(0;\nu\langle d\rangle^2\tau)P(1;\nu\langle d\rangle^2 d\tau) = \nu\langle d\rangle^2 e^{-\nu\langle d\rangle^2(\tau+d\tau)}d\tau \simeq \nu\langle d\rangle^2 e^{-\nu\langle d\rangle^2\tau}d\tau \quad (d\tau \sim 0). \tag{2}$$

In this case, the distribution function $f(\tau)$ is written as

$$f(\tau) = \nu\langle d\rangle^2 e^{-\nu\langle d\rangle^2\tau}.$$

A diamond crystal grows at a growth rate r within a time interval τ. One therefore obtains $d=r\tau$. Since r is a constant and $d\tau=dd/r$, using Eqs. (1) and (2), the distribution function of the crystal size $F(d)$ is given as

$$F(d) = \frac{\nu\langle d\rangle^2}{r}e^{-\nu\langle d\rangle^2/rd} = \frac{1}{\langle d\rangle}e^{-d/\langle d\rangle}.$$

The distribution function $F(d)$ is normalized since $f(\tau)$ is normalized.

As shown in Fig. 9(b), few diamond crystals smaller than 3 nm in diameter are present. This fact suggests the existence

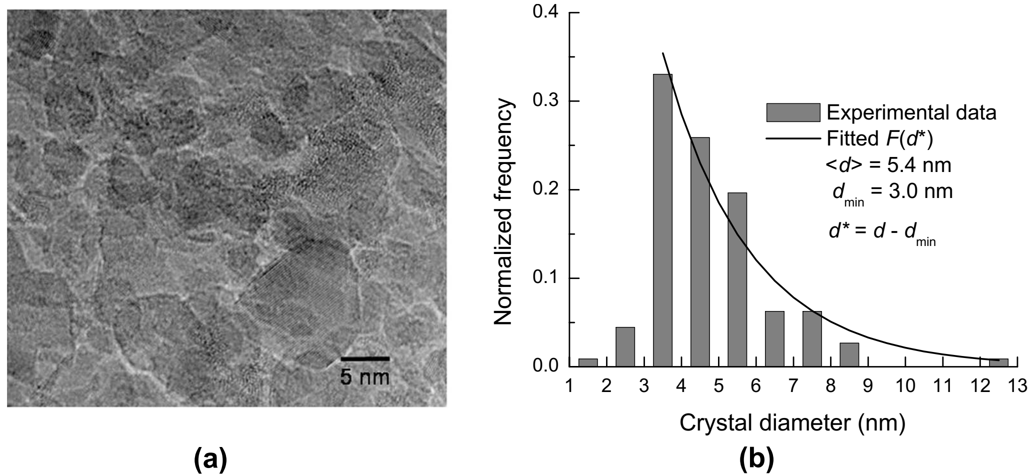

FIG. 9. TEM characterization to obtain the size distribution of diamond crystals. (a) A high-resolution TEM image of a NCD film on PPS. Diamond (111) lattice fringes are observed in some particles. (b) The size distribution of diamond crystals in the NCD film, the data of which were taken from the TEM image (a). Each frequency for respective crystal diameter is normalized by the total sample number of 112. The solid line indicates a theoretically derived distribution function of crystal size d, fitted to the experimental data.

of a minimum size of diamond crystals. Here the minimum diameter is defined as $d_{\min}$. Substitution of $d^*=d-d_{\min}$ for d yields a distribution function $F(d^*)$ as

$$F(d^*) = F(d - d_{\min}).$$

Fitting $F(d^*)$ to the experimental size distribution in Fig. 9(b) using $\langle d\rangle$ and $d_{\min}$ as fitting parameters, $\langle d\rangle=5.4$ nm and $d_{\min}=3.0$ nm have resulted in the best fit. As demonstrated in Fig. 9(b), $F(d^*)$, using $\langle d\rangle=5.4$ nm and $d_{\min}=3.0$ nm, reproduces the size distribution well. This value of $\langle d\rangle$ is quite close to the average crystallite size obtained from the x-ray diffraction (5.5 nm).

Diamond is a stable phase of carbon (more stable than graphite) at a pressure of over 2 GPa at room temperature. The pressure at which diamond is stable increases with increasing temperature.[27] The majority of commercially available synthetic diamonds are produced by high-pressure high-temperature process. In this process, diamonds grow in metal solvent such as Fe, Co, and Ni (Ref. 28) under a thermal equilibrium condition, for example, at a pressure of 5 GPa at 1500 °C. In this case, diamond is a thermodynamically stable phase.

On the other hand, responding to a demonstration of the presence of small diamonds (~5 nm) in meteorites,[29] Nuth[30] has pointed out the possibility that nanometer-sized diamond is stable in that particular size regime even at low pressures where a bulk diamond is metastable. In the size regime, thermodynamic predictions based on the bulk properties are not necessarily applicable to nanometer-sized particles. He attributed the reversal in the relative stability between diamond and graphite to increasing effect of surface free energy on the stability with decreasing dimensions of carbon particles.

By developing this discussion, more elaborated investigations into the stability of nanometer-sized diamond have been made to date.[31–36] Badziag *et al.*[31] have proceeded with the Nuth's discussion using a semiempirical quantum chemistry calculations. They concluded that diamonds of 3–5 nm in size are more stable than graphite regardless pressure or kinetics. Several other theoretical investigations have reached results of a similar peaked size distribution for diamond nanoparticles in a stable phase.[32–34,36] Raty and Galli,[34] in particular, have applied the discussion to the diamond CVD growth that requires the presence of hydrogen, using first-principles calculations. They found that the size distribution should exhibit a sharp peak at around 3 nm in the presence of hydrogen on the surfaces of diamond nanoparticles for a broad range of pressures and temperatures. They also suggested that diamonds start to grow from particles of this size to a film. In the present work, few crystals less than 3 nm are found in the crystal size distribution shown in Fig. 9(b), which indicates that the minimum size is 3 nm for our CVD process. In other words, the diamond crystals start to grow from 3 nm. This result supports these theoretical discussions.

In several experiments, nucleation of diamond in the gas phase at atmospheric or subatmospheric pressures has been observed.[37–41] Frenklach *et al.*[38] have extracted diamond aggregates from deposits collected from a microwave plasma without using any substrates. The aggregates typically exhibited 50 nm in diameter. They revealed that each aggregates consisted of many smaller diamond crystallites using selected-area electron diffraction. This is the evidence for the diamond nucleation in a stable phase in a microwave plasma.

Hwang *et al.*[35] have proposed a diamond CVD growth model by charged clusters. In elaborating the model theoretically, Jang and Hwang[36] have suggested remarkable reduction in the activation free energy for the diamond nucleation in the gas phase. They suggest that the diamond nucleation occurs in a plasma under certain conditions. They also demonstrated the existence of a broad but a deep potential-energy well for the cluster size larger than a critical size corresponding to the activation free energy. This implies that the nucleated diamond crystal in a plasma hardly transform into graphite.

The above discussion indicates the possibility of diamond nucleation in the gas phase under certain conditions. Once the gas-phase nucleation is assumed, the extremely low-temperature growth of diamond and the temperature dependences of the growth rate and the nucleation rate in the present work become understandable. That is to say, the substrate temperature is not responsible for the diamond nucleation in the gas phase. A nucleated diamond cluster in the plasma precipitates onto the substrate and grows there until another diamond cluster falls on it. The substrate temperature affects only the growth rate of the precipitated diamonds on the substrate. This assumption naturally leads to the NCD film growth at substrate temperature below 100 °C and the weak temperature dependence of the growth rate. Moreover, under the gas-phase nucleation, the substrate temperature is also considered not to be responsible for the nucleation rate. However, the nucleated diamonds are etched by atomic hydrogen and oxygen in the plasma, the rate of which increases with increasing substrate temperature. This explains the reciprocal temperature dependence of the nucleation rate.

In summarizing the foregoing discussion, we have reached the following model for the NCD growth in the surface-wave plasma. (1) Diamond crystals nucleate and grow into nuclei clusters of ~3 nm in size in the plasma. The diamond clusters precipitate on the substrate. (2) The precipitated clusters grow, or are removed by the hydrogen (oxygen) plasma etching, which depends on the substrate temperature.

The decreasing nucleation rate with increasing temperature in Fig. 8(a) is attributed to the increasing etching effect of the hydrogen (and also the oxygen) plasma on the clusters which increases with temperature. The nucleation in the plasma enables the low-temperature deposition of NCD films on plastic substrates at below 100 °C.

Dielectric particles in a plasma, such as the diamond clusters nucleated in the plasma, are bombarded by ions. The energy of the ions is proportional to the electron temperature of the plasma. The high-energy ion bombardment caused by a high electron temperature[13,42] blasts the nucleated diamonds in the plasma, viz., diamonds hardly nucleate in a high-electron-temperature plasma including conventional microwave plasmas for diamond growth (over 5 eV).[14,15] The low-electron temperature of the surface-wave plasma enables the gas-phase nucleation with a nucleation rate around $10^{10}/\mathrm{cm}^2\,\mathrm{s}$ [Fig. 8(a)] even in a hydrogen-rich plasma, whereas a conventional hydrogen-rich plasma reduces diamond renucleation, so that MCD films are grown.[25] Besides, the low-electron temperature suppresses excessive decomposition of carbon precursors, which causes nondiamond components in the deposited film. In brief, the low-electron temperature of the plasma is essential for the gas-phase nucleation in the low-temperature growth of diamond as well as for the reduction of the nondiamond-component formation. The gas-phase nucleation is indispensable for the diamond deposition at such low temperatures.

V. SUMMARY

Using low pressures of the reaction gas and a microwave surface-wave plasma with a low-electron temperature, NCD films have been grown on plastic (PPS) substrates at substrate temperatures below 100 °C. Raman-scattering spectra of the films indicate diamond film formation under such low substrate temperatures. X-ray diffraction and TEM observation reveal that the average diamond crystal size of the film is around 5 nm. An analysis of the temperature dependence of growth rates and nucleation rates suggests a different growth mechanism from that in usual diamond growth. Moreover, an analysis of the size distribution of diamond crystals in the film implies diamond nucleation in a stable phase in the plasma, which is invoked by the low-electron temperature of the surface-wave plasma. The gas-phase nucleation enables an explanation on the mechanism of the low-temperature growth of NCD films on plastic substrates in the present work.

ACKNOWLEDGMENTS

This work was supported by a grant Nano-diamond coating for injection molded PPS (Research and Development of Nanodevices for Practical Utilization of Nanotechnology) from the New Energy and Industrial Technology Development Organization (NEDO), Japan. This work was partially supported by a grant "Creation of New Materials by Nanocrystalline Diamond Film Coating" (Grant No. AS2112903C) of Adaptable and Seamless Technology Transfer Program through target-driven R&D (ASTEP) from Japan Science and Technology Agency (JST). The authors acknowledge S. Kawaki of AIST for his support to the CVD growth process operations in this work. The authors also acknowledge H. Sakakita and H. Koguchi of AIST for their support to the plasma diagnosis in the present work.

*k.tsugawa@aist.go.jp
†hasegawa.masataka@aist.go.jp

[1] A. Aleksov, X. Li, N. Govindaraju, J. M. Gobien, S. D. Wolter, J. T. Prater, and Z. Sitar, Diamond Relat. Mater. **14**, 308 (2005); J.-P. Mazellier, J. Widiez, F. Andrieu, M. Lions, S. Saada, M. Hasegawa, K. Tsugawa, L. Brevard, J. Dechamp, M. Rabarot, V. Delaye, S. Cristoloveanu, L. Clavelier, S. Deleonibus, P. Bergonzo, and O. Faynot, 2009 IEEE Int. SOI Conf., 141 (2009).
[2] J. C. Angus and C. C. Hayman, Science **241**, 913 (1988).
[3] T. G. McCauley, D. M. Gruen, and A. R. Krauss, Appl. Phys. Lett. **73**, 1646 (1998).
[4] T. P. Ong and R. P. H. Chang, Appl. Phys. Lett. **55**, 2063 (1989).
[5] Y. Muranaka, H. Yamashita, and H. Miyadera, J. Appl. Phys. **69**, 8145 (1991).
[6] M. Ihara, H. Maeno, K. Miyamoto, and H. Komiyama, Appl. Phys. Lett. **59**, 1473 (1991).
[7] T. Yara, H. Makita, A. Hatta, T. Ito, and A. Hiraki, Jpn. J. Appl. Phys., Part 2 **34**, L312 (1995).

[8] F. Piazza and G. Morell, Diamond Relat. Mater. **16**, 1950 (2007).
[9] K. Tsugawa, M. Ishihara, J. Kim, M. Hasegawa, and Y. Koga, New Diamond Front. Carbon Technol. **16**, 337 (2006).
[10] K. Tsugawa, M. Ishihara, J. Kim, Y. Koga, and M. Hasegawa, J. Phys. Chem. C **114**, 3822 (2010).
[11] H. Sugai, I. Ghanashev, and M. Nagatsu, Plasma Sources Sci. Technol. **7**, 192 (1998).
[12] H. Sugai, I. Ghanashev, and K. Mizuno, Appl. Phys. Lett. **77**, 3523 (2000).
[13] J. Kim and M. Katsurai, J. Appl. Phys. **101**, 023301 (2007).
[14] F. M. Cerio and W. A. Weimer, Appl. Phys. Lett. **59**, 3387 (1991).
[15] T. Sharda, G. S. Misra, D. K. Avasthi, and G. K. Mehta, Solid State Commun. **98**, 879 (1996).
[16] T. Anthony, Vacuum **41**, 1356 (1990).
[17] T. Kawato and K. Kondo, Jpn. J. Appl. Phys., Part 1 **26**, 1429 (1987).
[18] A. Inspektor, Y. Liou, T. McKenna, and R. Messier, Surf. Coat. Technol. **39-40**, 211 (1989).
[19] D. Das, R. N. Singh, I. T. Barney, A. G. Jackson, and M. Mukhopadhyay, J. Vac. Sci. Technol. A **26**, 1487 (2008).
[20] H. P. Klug and A. L. Elbert, *X-Ray Diffraction Procedures for Polycrystalline and Amorphous Materials*, 2nd ed. (Wiley, New York, 1974), Chap. 9.
[21] R. A. Young and D. B. Wiles, J. Appl. Crystallogr. **15**, 430 (1982).
[22] E. Kondoh, T. Ohta, T. Mitomo, and K. Ohtsuka, Appl. Phys. Lett. **59**, 488 (1991); J. Appl. Phys. **73**, 3041 (1993).
[23] C. J. Chu, R. H. Hauge, J. L. Margrave, and M. P. D'Evelyn, Appl. Phys. Lett. **61**, 1393 (1992).
[24] J. Robertson, Phys. Status Solidi A **205**, 2233 (2008).
[25] O. A. Williams, M. Nesladek, M. Daenen, S. Michaelson, A. Hoffman, E. Osawa, K. Haenen, and R. B. Jackman, Diamond Relat. Mater. **17**, 1080 (2008).
[26] D. C. Barbosa, F. A. Almeida, R. F. Silva, N. G. Ferreira, V. J. Trava-Airoldi, and E. J. Corat, Diamond Relat. Mater. **18**, 1283 (2009).
[27] F. P. Bundy, H. P. Bovenkerk, H. M. Strong, and R. H. Wentorf, Jr., J. Phys. Chem. **35**, 383 (1961).
[28] H. P. Bovenkerk, F. P. Bundy, H. T. Hall, H. M. Strong, and R. H. Wentorf, Jr., Nature (London) **184**, 1094 (1959).
[29] R. S. Lewis, T. Ming, J. F. Wacker, E. Anders, and E. Steel, Nature (London) **326**, 160 (1987).
[30] J. A. Nuth III, Nature (London) **329**, 589 (1987).
[31] P. Badziag, W. S. Verwoerd, W. P. Ellis, and N. R. Greiner, Nature (London) **343**, 244 (1990).
[32] M. Y. Gamarnik, Phys. Rev. B **54**, 2150 (1996).
[33] A. S. Barnard, S. P. Russo, and I. K. Snook, Phys. Rev. B **68**, 073406 (2003).
[34] J. Y. Raty and G. Galli, Nature Mater. **2**, 792 (2003).
[35] N. M. Hwang, J. H. Hahn, and D. Y. Yoon, J. Cryst. Growth **162**, 55 (1996); N. M. Hwang, *ibid.* **198-199**, 945 (1999).
[36] H. M. Jang and N. M. Hwang, J. Mater. Res. **13**, 3527 (1998); **13**, 3536 (1998).
[37] S. Mitura, J. Cryst. Growth **80**, 417 (1987).
[38] M. Frenklach, R. Kematick, D. Huang, W. Howard, K. E. Spear, A. W. Phelps, and R. Koba, J. Appl. Phys. **66**, 395 (1989).
[39] W. Howard, D. Huang, J. Yuan, M. Frenklach, K. E. Spear, R. Koba, and A. W. Phelps, J. Appl. Phys. **68**, 1247 (1990).
[40] P. R. Buerki and S. Leutwyler, J. Appl. Phys. **69**, 3739 (1991).
[41] M. Frenklach, W. Howard, D. Huang, J. Yuan, K. E. Spear, and R. Koba, Appl. Phys. Lett. **59**, 546 (1991).
[42] J. Kim, K. Tsugawa, M. Ishihara, Y. Koga, and M. Hasegawa, Plasma Sources Sci. Technol. **19**, 015003 (2010).